4-1-2009

Thermal stability and flammability characteristics of ethylene vinyl acetate (EVA) composites blended with a phenyl phosphonate-intercalated layered double hydroxide (LDH), melamine polyphosphate and/or boric acid

Calistor Nyambo
Marquette University

Everson Kandare
University of Bolton

Charles A. Wilkie
Marquette University, charles.wilkie@marquette.edu

Accepted version. *Polymer Degradation and Stability*, Vol. 94, No. 4 (April 2009): 513-520. DOI.

Polymer Degradation and Stability, Vol. 94, No. 4 (April 2009): 513-520. DOI.

Thermal Stability and Flammability Characteristics of Ethylene Vinyl Acetate (EVA) Composites Blended with A Phenyl Phosphonate-Intercalated Layered Double Hydroxide (LDH), Melamine Polyphosphate And/Or Boric Acid

Calistor Nyambo
Department of Chemistry and Fire Retardant Research Facility, Marquette University, Milwaukee, WI
Everson Kandare
Centre for Materials Research and Innovation, University of Bolton, BL3 5AB, UK
Charles A. Wilkie
Department of Chemistry and Fire Retardant Research Facility, Marquette University, Milwaukee, WI

Abstract

A phenyl phosphonate-intercalated MgAl–LDH (MgAl–PPh), melamine polyphosphate (MP), and boric acid (BA) were independently and concomitantly added to neat ethylene vinyl acetate (EVA) copolymer at loading fractions of 10% (w/w). The structural morphology of MgAl–PPh was established via powder X-ray diffraction

(PXRD) and scanning electron microscopy (SEM) while the presence of phenyl phosphonate in the galleries was confirmed by Fourier transform infrared (FTIR). Thermogravimetric analysis (TGA) and cone calorimetry were used to evaluate the thermal stability and flammability behavior of EVA and its composites. While time-to-ignition is greatly reduced for EVA composites compared to the virgin polymer, there are remarkable reductions in the peak heat release rate (PHRR) which relates to a reduction in flame intensity. Synergistic effects were observed in cone calorimetry for the formulation containing MgAl–PPh, MP, and BA.

Keywords

EVA, Layered double hydroxide, Melamine polyphosphate, Boric acid, Synergy

1. Introduction

Ethylene vinyl acetate (EVA) copolymer is readily available in the form of rubber, thermoplastic elastomers, and plastic and is widely used in the wire and cable industry due to its desirable physico-chemical properties and its easy acceptance of additives [1]. The ease of ignition and subsequent flaming combustion with the release of large volumes of toxic smoke prohibit the application of EVA-based materials in high temperature service environments. A plausible solution to this problem is the addition of flame retardant additives which may improve the fire safety of EVA-based materials. Non-halogenated flame retardant additives, such as intumescent systems [2], [3], carbon nanotubes [4], [5], modified natural cationic clays [6], metal hydroxides [7], and oxides of group III and V elements [8]have been widely utilized with EVA. However, more recently synthetic clays, known as layered double hydroxides (LDH), have been used with EVA and do show flame retardancy potential [9], [10], [11], [12].

Layered double hydroxides are lamellar structured hydrotalcite-like compounds with anionic exchange properties similar to the extensively studied cationic clays such as montimorillonite. Their generic formula is $[M_{1-x}^{2+}M_x^{3+}(OH)_2]^{x+}A_{x/m}^{n-}\cdot nH_2O$, where M^{2+} and M^{3+} are divalent and trivalent metal cations, such as Mg^{2+} and Al^{3+}, respectively, and A^{n-} is interlayer anion, which is exchangeable such as NO_3^-, CO_3^{2-}, and PO_4^{3-}. The ability to exchange the interlayer anions introduces a fascinating design opportunity via which known potential flame retardant anions can be incorporated into the lamellar structure before adding the LDH to a polymer matrix. While magnesium hydroxide, aluminum hydroxide, and phosphorus-containing compounds have been extensively studied independently as flame retardant additives, their flame retardation efficiency in EVA may be improved by designing a phosphonate-intercalated MgAl–LDH which may prevent premature decomposition of phosphorus-containing additives. The anticipated water vapor from dehydroxylation of intralayer structures and the release of phosphorus derivatives during decomposition may decrease the amount of combustible volatiles while promoting char formation and subsequently inhibiting heat and mass transfer.
In the present study, we have explored the effect of a phosphonate-intercalated MgAl–LDH (MgAl–PPh) on the thermal and flammability behavior of EVA using thermogravimetric analysis (TGA) and cone calorimetry. Flame retardant/EVA blends containing MgAl–PPh and of 10% were also studied and compared to EVA composites containing MgAl–PPh.

2. Experimental

2.1. Materials

Magnesium nitrate hexahydrate, $Mg(NO_3)_2\cdot 6H_2O$, aluminum nitrate nonahydrate, $Al(NO_3)_3\cdot 9H_2O$, sodium hydroxide flakes, NaOH and glycerol (Aldrich Chemical Co.), phenyl phosphonic acid [PPh], ($C_6H_5PO(OH)_2$) (TCI), ethylene vinyl acetate copolymer, [EVA], (Escorene Ultra EVA UL 00218CC3 from Exxon Mobil Chemical), boric acid [BA] Rio Tinto Inc., melamine polyphosphate (melapur 200/70®, [MP] (Ciba Specialty Chemicals)) were used as-received without further purification. Hydrotalcite, (pural MG63HT), referred herein as MgAl–carbonate LDH, was kindly provided by Sasol Germany, GmbH.

2.2. Preparation of MgAl–phenyl phosphate layered double hydroxide (MgAl–PPh LDH)

The phenyl phosphonate intercalated MgAl–LDH (referred hereafter as MgAl–PPh) was prepared by rehydration of the calcined hydrotalcite (MgAl–carbonate) following a procedure reported by Dimotakis and Pinnavaia [13]. In a typical experiment, the MgAl–carbonate LDH was calcined in air at 450 ± 10 °C for 18 h. 1.0 g of the calcined material was then added to phenyl phosphonate solution (0.1 M; 100 mL) prepared by dissolving phenyl phosphonic acid in a 0.2 M solution of NaOH in water/glycerol (1:2 v/v) under a steady flow of nitrogen to exclude carbon dioxide at 50 °C. It is imperative that CO_2 is excluded since its presence will lead to the formation of a carbonate. The resulting slurry was aged at 50 °C for 24 h, filtered and washed several times with hot deionized/degassed water followed by drying at 100 °C in a vacuum oven.

2.3. Preparation of EVA/LDH/melamine polyphosphate/boric acid composites

Ethylene vinyl acetate composites were prepared via melt blending using established literature methods [14]. Melt blending was performed in a Brabender mixer at a temperature of 130 °C at a screw speed of 60 rpm for 8 min. EVA composite samples were prepared by adding predetermined additive weight fractions of the hydrotalcite, MP, and/or BA to a measured portion of the copolymer in order to achieve a cumulative additive fraction of 10% (w/w). The constitutive proportions of EVA formulations are shown in Table 1. A reference sample of unmodified EVA was obtained by following the same procedure only without any additive.

Table 1. Composition of EVA composites.

Sample	EVA (%)	MgAl–PPh (%)	MP (%)	BA (%)
EVA	100	0	0	0
EVA/BA-10	90	0	0	10
EVA/MP-10	90	0	10	0
EVA/MgAl–PPh-10	90	10	0	0
EVA/MgAl–PPh/MP/BA-2/4/4	90	2	4	4
EVA/MgAl–PPh/MP/BA-4/2/4	90	4	2	4
EVA/MgAl–PPh/MP/BA-4/4/2	90	4	4	2

2.4. Instrumentation

Powder X-ray diffraction measurements (PXRD) of the LDHs, char and their calcination products were recorded on a Rigaku, Miniflex II Desktop, X-ray diffractometer with Cu (K_α) source λ = 1.54078 Å, from a sealed X-ray tube. The powdered samples were prepared and mounted on a glass holder while thin plaques of composites were fabricated via compression molding and mounted on aluminum sample holder. The data were collected at 2ϑ values of 0–60° at a scan rate of 0.0833 °/s with a sampling width of 0.02. Basal spacing of LDHs was obtained from averaging 00*l* reflections (*l* = 3, 6, 9).

The scanning electron microcopy (SEM) image of the layered double hydroxide (MgAl–BP) was obtained via a Cambridge Stereoscan 200 with the sample coated with a conductive layer of gold.
Fourier transform infrared spectra of layered double hydroxides and their respective calcined products were obtained using the KBr disk method on a Nicolet Magna-IR 560 spectrometer operating at 1 cm^{-1}resolution in the 400–4000 cm^{-1} region.

Thermogravimetric analysis, (TGA) and differential thermal analysis (DTA) were performed on an SDT 2960 simultaneous DTA–TGA instrument from 50 to 800 °C at a heating rate of 20 °C/min in N_2, flowing at 85 ± 5 mL/min, with sample sizes of 15.0 ± 1.0 mg contained in aluminum sample cups. All samples were run in triplicate and average values are reported; temperatures are considered accurate to ±3 °C and the error on the fraction of non-volatile materials is ±2%. Calcination of the hydrotalcite, MgAl–carbonate was performed in a Thermolyne 1300 furnace at 450 °C for 18 h.

Approximately 30 g of EVA composite specimens were compression molded into 100 mm × 100 mm square plaques of uniform thickness (~3 mm) before cone calorimetry was performed on an Atlas Cone 2 instrument according to ASTM E 1354 at an incident flux of 35 kW/m^2 with a cone shaped heater; the spark was continuous until the sample ignited. All samples were run in triplicate and the average value, with standard deviation, is reported; results from cone calorimeter are generally considered to be reproducible to ±10%.

3. Results and discussion

3.1. Structural characterization of the LDHs and their EVA composites

3.1.1. Infrared and X-ray diffraction analysis

Fig. 1 shows the powder X-ray diffraction (PXRD) patterns of the precursor layered double hydroxide, MgAl–carbonate, its calcined product, and the phenyl phosphonate intercalated hydrotalcite, MgAl–PPh. PXRD patterns of MgAl–carbonate reveal narrow and equidistantly spaced 00*l* (*l* = 3, 6, 9) basal reflections in the low angle region leaving no doubt that these materials are layered and possess a high degree of ordering in the *c* dimension. Analysis of the positions of 00*l* peaks using the Bragg equation gives an average *d* spacing of 7.4 Å. The PXRD pattern of the calcined hydrotalcite shows no basal reflections over the whole scanned range indicative of the possible presence of an amorphous mixture of Mg and Al oxides [15]. Upon re-hydration of the calcined phase with an aqueous solution containing phenyl phosphonate the layered structure was recovered. The resultant product, MgAl–PPh, exhibits strong and sharp 00*l* basal reflections indicative of well-crystallized layered phases and its basal spacing is calculated to be 13.8 Å which is twice that of MgAl–carbonate. The layered structure of MgAl–PPh is confirmed by the scanning electron microscopy images. The SEM image, Fig. 2, shows that MgAl–PPh is composed mainly of plate-like particles with sharp edges stacked upon each other. No change in *d* spacing was observed when MgAl–PPh LDH was combined with the EVA as shown by the XRD traces presented in Fig. 3. This observation indicates that a microcomposite has been formed.

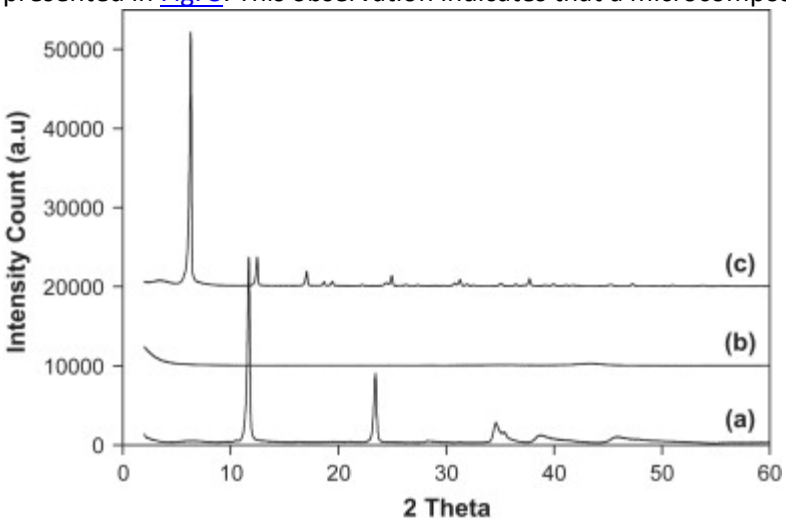

Fig. 1. Powder XRD pattern of (a) MgAl–carbonate, (b) MgAl–carbonate calcined at 450 °C for 18 h, and (c) MgAl–PPh layered double hydroxide. Data are offset for clarity but not otherwise scaled.

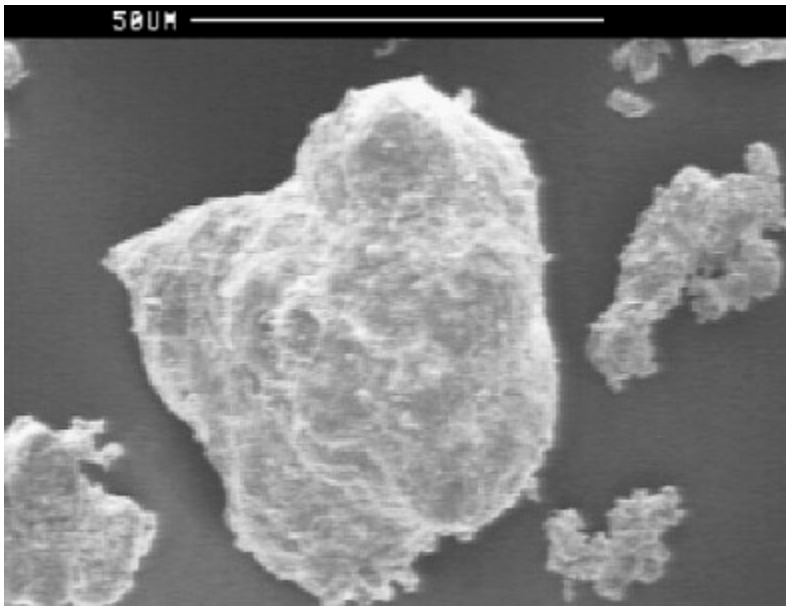

Fig. 2. The SEM image of MgAl–PPh layered double hydroxide.

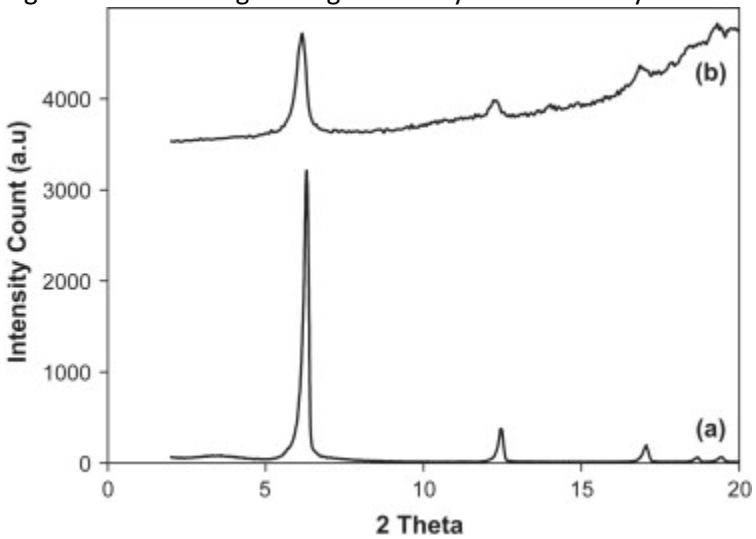

Fig. 3. The XRD patterns of (a) MgAl–PPh layered double hydroxide and (b) EVA/MgAl–PPh-10 composite.

The FT-IR spectra of MgAl–carbonate and MgAl–PPh shown in Fig. 4 reveal the characteristic absorption bands of hydrotalcite-like compounds. Both MgAl–carbonate and MgAl–PPh show the absorption bands from O–H stretching at about 3500 cm^{-1}, δ (H–OH) vibrations at about 1640 cm^{-1}, and the lattice vibration of the M–O and O–M–O (M = Mg and Al) groups in the low frequency region below 800 cm^{-1} [9]. The absorption bands at 1370 and 1060 cm^{-1} in the spectrum of MgAl–carbonate are assigned to the carbonate stretching. For the phosphonate intercalated LDH, MgAl–PPh, characteristic absorption peaks of phenyl phosphonate are evident; (i) 1443 cm^{-1}: sharp P–C stretching vibration, (ii) 1150, 1110, and 1018 cm^{-1}: vibrations of the O_3P–C group, and (iii) 762, 733, and 702 cm^{-1}(medium intensity): characteristic bands of the mono-substituted phenyl ring [16]. An absorption band at 1406 cm^{-1} also present in the FT-IR spectrum of the calcined MgAl–carbonate LDH may be due to free carbonates due residual carbonate after calcination or from atmospheric contamination which is hard to prevent.

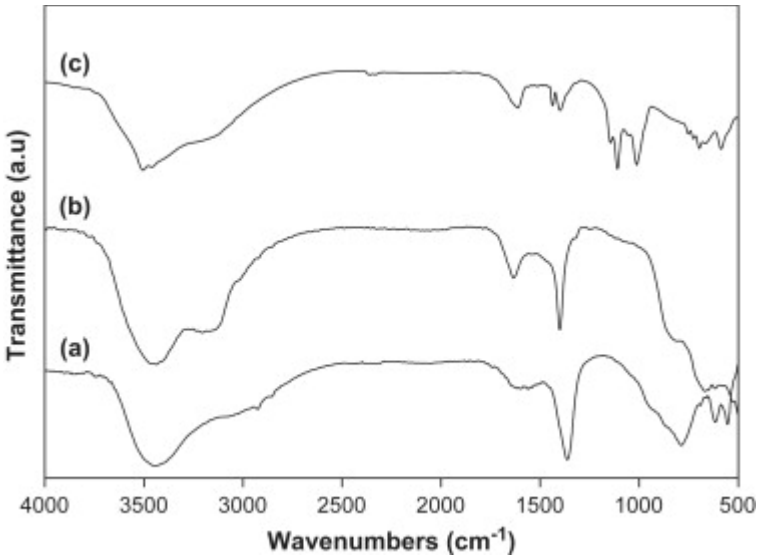

Fig. 4. FTIR spectra of (a) MgAl–carbonate, (b) MgAl–carbonate calcined at 450 °C for 18 h, and (c) MgAl–PPh layered double hydroxide. Spectra are offset for clarity.

3.2. Thermal stability of potential flame retardants and their EVA composites

3.2.1. Thermal degradation behavior of potential flame retardant additives

Fig. 5 shows the TGA mass loss profiles of the potential flame retardant additives MgAl–PPh, melamine polyphosphate, and boric acid in an inert atmosphere. The thermal degradation of MgAl–PPh displays a four-step process in the temperature range of 50–800 °C. The first two steps, occurring between 60 and 250 °C, may be due to the loss of water of hydration and intercalated water molecules equivalent to 13% of the LDH. The third step occurs between 300 and 500 °C and is probably due to dehydroxylation of the –MgAl–OH– intralayer structure while the fourth and most prominent step between 500 and 600 °C may be attributed to deanation as reported in previous work [17], [18], [19]. The production of water vapor, the presence of phosphate, and formation of metal oxides during the thermal degradation of the layered double hydroxide may serve to improve the thermal stability of EVA/MgAl–PPh blends via: (i) cooling of the specimen environment by water vapor, (ii) formation of charred layers that may be promoted by the chemical interactions between polymeric fragments and phosphate derivatives [20], and (iii) catalytic chemical activities that may slow the scission of polymer chains while promoting fragment recombinations.

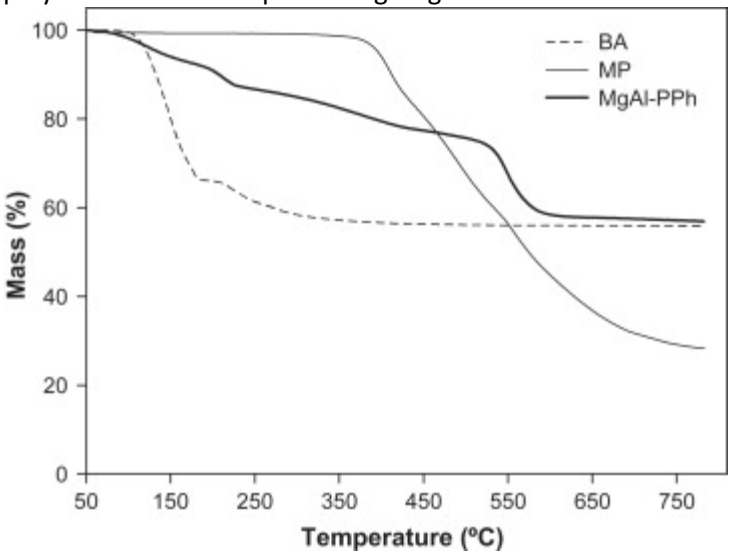

Fig. 5. TGA curves for boric acid (dashed line), melamine polyphosphate (solid line) and MgAl–PPh (bold line) at 20 °C/min under a N_2 atmosphere.

From the TGA curve in Fig. 5, it can be seen that melamine polyphosphate does not show any significant weight loss at temperatures below 400 °C. However, above this temperature, melamine polyphosphate undergoes an endothermic decomposition process releasing melamine which subsequently sublimes or degrades, releasing ammonium and water [21]. The phosphate is converted into phosphoric acid and polyphosphoric acids which may promote the formation of residual char in the condensed phase [22]; the char yield of MP at 800 °C is 28%. The thermal degradation of boric acid, Fig. 5, follows a two-step mechanism: the first step between 100 and 180 °C, corresponding to a weight loss of 34%, is due to the dehydration of boric acid into metaboric acid, HBO_2 while the second step with a mass loss of 10% between 180 and 400 °C, may be attributed to the dehydration of HBO_2 into boron oxide, B_2O_3, leaving 56% residual char. Such high levels of residual char in the form of "hard glass", B_2O_3, are imperative in the formation of the ultimate physical barrier with a high structural integrity [23].

3.2.2. Thermogravimetric behavior of EVA and its composites

The TGA curves for unmodified EVA and its MP, BA, and, MgAl–PPh composites are shown in Fig. 6while the data are presented in Table 2. The mass loss profile of EVA shows a two stage degradation pathway with the first step attributed to the elimination of acetate side groups (deacetylation) leaving behind an unsaturated polymer backbone or polyene [24], [25], [26], while the second step is due to the allylic chain scission of the polyene to reach full thermal degradation at high temperatures [27]. The onset of thermal degradation for unmodified EVA, measured as the temperature at which 10% mass loss occurs, T_{10}, is 351 °C while T_{max}, the temperature at which maximum mass loss occurs, is 456 °C. The addition of BA, MP, and MgAl–PPh at a loading fraction of 10% by weight leads to the shift in degradation processes to higher temperatures.

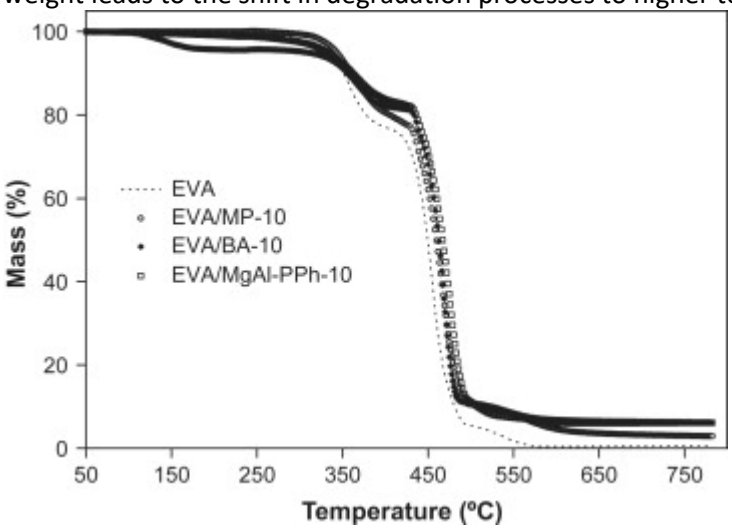

Fig. 6. TGA curves for neat EVA (dotted line), EVA/MP-10 (filled circles), EVA/BA-10 (filled diamonds), and EVA/MgAl–PPh-10 (empty squares) at 20 °C/min under a N_2 atmosphere.

Table 2. TGA data for flame-retarded EVA formulations.

Sample	**T_{10}(°C)**	**ΔT_{10}(°C)**	**OSE (%)**	**Char at 800 °C (%)**	**TGA 1st stage**		**TGA 2nd stage**	
					Temp. range (°C)	**Peak pos.; (peak max.)[a](°C); (% °C^{-1})**	**Temp. range (°C)**	**Peak pos.; (peak max.)[a](°C); (% °C^{-1})**
EVA	351	–	–	1	240–400	358; (*0.5*)	400–500	456; (*2.1*)
EVA/BA-10	355	4	1503	6	240–415	363; (*0.3*)	415–500	468; (*2.5*)

EVA/MP-10	360	9	1402	3	240–415	360; (*0.3*)	415–500	468; (*1.7*)
EVA/MgAl–PPh-10	361	10	1939	6	240–410	366; (*0.2*)	410–500	476; (*1.8*)
EVA/MgAl–PPh/MP/BA-2/4/4	364	13	1337	5	240–415	363; (*0.3*)	415–500	470; (*2.2*)
EVA/MgAl–PPh/MP/BA-4/2/4	364	13	1835	6	240–415	369; (*0.3*)	415–500	471; (*2.0*)
EVA/MgAl–PPh/MP/BA-4/4/2	364	13	1614	5	240–415	365; (*0.3*)	415–500	469; (*2.4*)

[a] Peak max. is the derivatized thermal degradation (DTG) response/signal value at the peak position while Peak pos. is the peak location with respect to temperature.

The addition of MP to EVA at 10% weight fraction leads to a slight delay in the thermal degradation processes of EVA as shown in Fig. 6. The onset of thermal degradation, T_{10}, is increased by 9 °C; the temperature at which the maximum mass loss rate recorded is increased from 456 to 468 °C and the residual char yield slightly increased by 2.3%. At temperatures above 400 °C, melamine polyphosphate undergoes endothermic decomposition releasing melamine, which subsequently sublimes or decomposes into incombustible NH_3; this process acts as a heat sink cooling the specimen. The release of phosphate derivatives may lead to the formation of phosphoric acids which are known to promote char formation, therefore shielding the condensed combustible polymer. The interaction between the envisaged degradation products of MP such as melamine, NH_3, phosphoric acids, and those of EVA induces the shift in degradation temperatures observed. However, the observed shift in degradation temperatures and the residual char at 800 °C are no more than the calculated values, suggesting that while MP antagonistically delays the degradation process in the lower temperature regime eventually all the polymer matrix degrades at higher temperatures.

The thermal degradation profile of EVA/BA composite, shown in Fig. 6, suggests that the addition of boric acid leads to the destabilization of EVA in the lower temperature regime (100–350 °C). Boric acid degrades to form B_2O_3 releasing water as discussed above. The calculated mass loss from boric acid of 4.4% at temperatures below 350 °C attributed to the loss of water vapor agrees very well with the observed mass loss of 4.3% observed in Fig. 6. H_3BO_3 loses water below 350 °C and the resultant probable product, B_2O_3, is expected to improve the thermal stability of EVA at higher temperatures. The onset of thermal degradation, T_{10}, is slightly increased by 4 °C; the temperature at which the maximum mass loss rate is recorded is increased from 456 to 468 °C and the residual char yield increased by 5.5%.

The addition of a phosphonate intercalated hydrotalcite-like LDH, MgAl–PPh, influences the thermal degradation of EVA more than MP or BA, Fig. 6. EVA/MgAl–PPh-10 follows the degradation pattern similar to that of EVA but the degradation temperatures are elevated. The onset of thermal degradation is enhanced by 10 °C while the temperature at which decomposition occurs at the maximum rate is increased by 20 °C relative to EVA. The shift in degradation temperatures may be attributed to the evolution of water, the presence of phosphate derivatives, and the probable catalytic effect due to the formation of mixed metal oxides during the thermal degradation of MgAl–PPh. MgAl–PPh may act via its decomposition to promote char formation thus protecting the underlying polymer hence decreasing the rate of degradation of EVA.

Mass difference curves, Δ mass% (mass% of EVA composites minus mass% of unmodified EVA at the same temperature) for EVA/BA-10, EVA/MP-10, and EVA/MgAl–PPh-10 composites are shown in Fig. 7. Positive Δ mass% profiles are indicative of enhancement in thermal stability of EVA following addition of the additives

while negative Δ mass% imply an adverse effect of the additives on the thermal stability of the polymer matrix. Boric acid greatly compromises the thermal stability of EVA at temperatures below 350 °C; but, it promotes char formation at higher temperatures, perhaps due to the presence of the heat resistant B_2O_3. A slight destabilization effect is observed below 350 °C for EVA/MgAl–PPh-10 while the addition of MP has no adverse effect on the thermal stability of EVA over the entire temperature range. While MP does not lower the thermal stability of EVA at low temperatures, it also does not effectively promote char formation as boric acid and MgAl–PPh do.

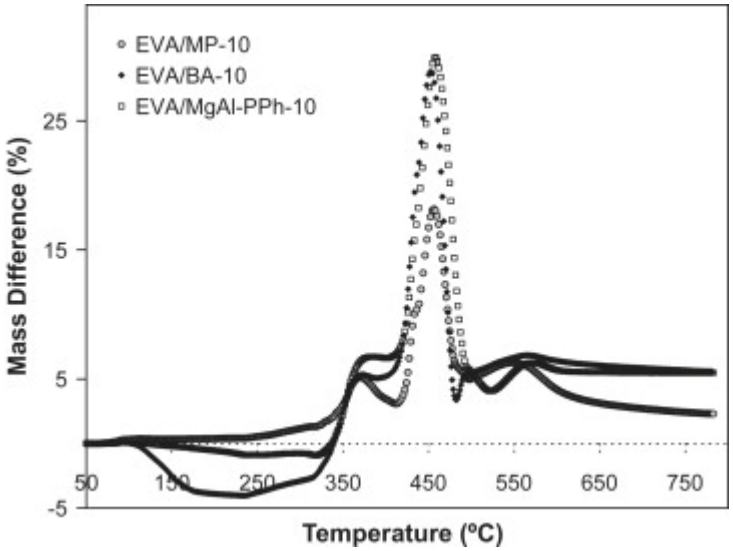

Fig. 7. Curves of mass loss differences as a function of degradation temperature for EVA composites at 10% loadings; EVA/MP-10 (filled circles), EVA/BA-10 (filled diamonds), and EVA/MgAl–PPh-10 (empty squares).

A quantitative assessment of the overall thermal stabilization effect (OSE) of BA, MP, and MgAl–PPh was evaluated using an established method in literature [17]. The OSE values are positive for all three composites suggesting that at 10% additive fraction all the additives do enhance the overall thermal stability of EVA over the temperature region studied. The calculated OSE values for EVA/BA-10, EVA/MP-10, and EVA/MgAl–PPh-10 are 1503, 1402, and 1939% respectively. These values suggest that MgAl–PPh is more effective at improving the thermal stability of EVA than boric acid or melamine polyphosphate. The release of water vapor, phosphate derivatives, and the presence of mixed oxides during the thermal degradation of EVA/MgAl–PPh-10 may serve to enhance the thermal stability of EVA via different pathways including; (i) the presence of endothermic heat sinks, (ii) promotion of char formation due to the presence of phosphorus derivatives in the condensed phase, (iii) chemical interactions of polymer fragments with or over mixed metal oxides.

Fig. 8 shows the thermal degradation of EVA composites containing all three additives used simultaneously at a cumulative additive fraction of 10% (EVA/MgAl–PPh/MP/BA-2/4/4, EVA/MgAl–PPh/MP/BA-4/2/4, and EVA/MgAl–PPh/MP/BA-4/4/2) while the data are presented in Table 2. The TGA profiles of these composites are similar and are shifted to higher degradation temperatures relative to EVA. The onset of degradation for these three composites occurs at a temperature of 364 °C which is an increase of 13 °C relative to EVA. The maximum mass loss rate occurs at approximately 470 °C for all three samples, a significant increase from 456 °C recorded for the control sample, EVA.

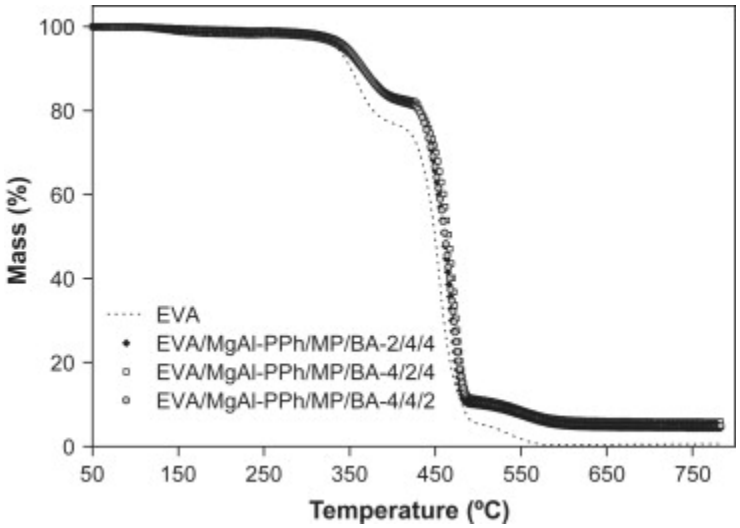

Fig. 8. TGA curves for neat EVA (dotted line), EVA/MgAl–PPh/MP/BA-2/4/4 (filled diamonds), EVA/MgAl–PPh/MP/BA-4/2/4 (empty squares), and EVA/MgAl–PPh/MP/BA-4/4/2 (filled circles) at 20 °C/min under a N_2atmosphere.

Mass difference curves of these three samples, Fig. 9, show a slight destabilization effect in the temperature region below 350 °C. While the patterns for mass difference curves are similar, EVA/MgAl–PPh/MP/BA-4/2/4 is the most thermally stabilized in the temperature region where the fastest rate of mass loss occurs. The calculated OSE values for EVA/MgAl–PPh/MP/BA-2/4/4, EVA/MgAl–PPh/MP/BA-4/2/4, and EVA/MgAl–PPh/MP/BA-4/4/2 are 1337, 1835, and 1614% respectively. These values suggest the following order of thermal stability in accordance with OSE values: EVA/MgAl–PPh/MP/BA-2/4/4 < EVA/MP-10 < EVA/BA-10 < EVA/MgAl–PPh/MP/BA-4/4/2 < EVA/MgAl–PPh/MP/BA-4/2/4 < EVA/MgAl–PPh-10. From these data, it may be concluded that MgAl–PPh has the most thermal stabilization effect while EVA/MgAl–PPh/MP/BA-2/4/4 is the least stabilized composite.

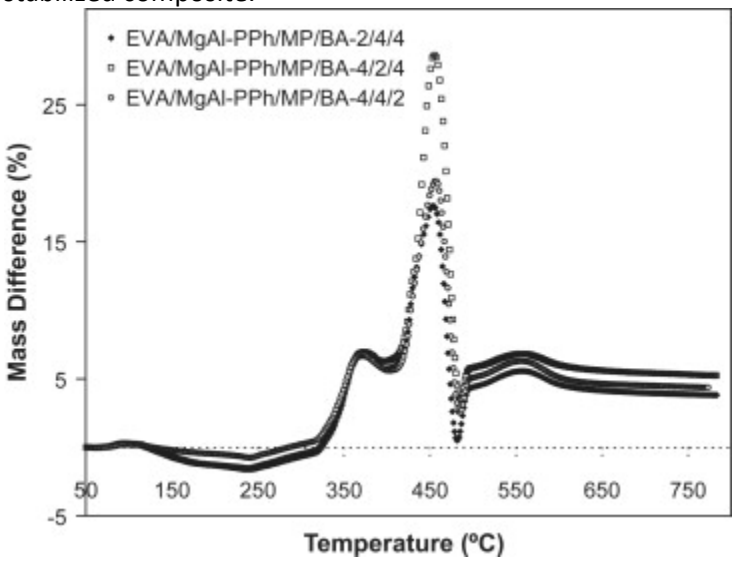

Fig. 9. Curves of mass loss differences as a function of degradation temperature for EVA composites at 10% loadings; EVA/MgAl–PPh/MP/BA-2/4/4 (filled diamonds), EVA/MgAl–PPh/MP/BA-4/2/4 (empty squares), and EVA/MgAl–PPh/MP/BA-4/4/2 (filled circles).

3.3. Flammability characterization of EVA and its composites

Cone calorimetry was used to evaluate the flammability behavior of EVA and its composites. Various parameters obtained or derived from experimental cone calorimetry results can be correlated to large-scale fire tests which are used to predict the burning behavior of materials in real fire scenarios. Fig. 10 shows the heat release rate

(HRR) versus time curves for EVA, EVA/BA-10, EVA/MP-10, and EVA/MgAl–PPh-10 and the data are presented in Table 3 and the plots of total heat release (THR) as a function of time for EVA are shown in Fig. 11. The fire growth index (FIGRA) used as a flame spread indicator parameter is calculated as the ratio of PHRR to the time-to-PHRR. The lower the FIGRA value the higher the fire safety of a given material. The FIGRA value for EVA is calculated as 8.2 kW/m^2 s.

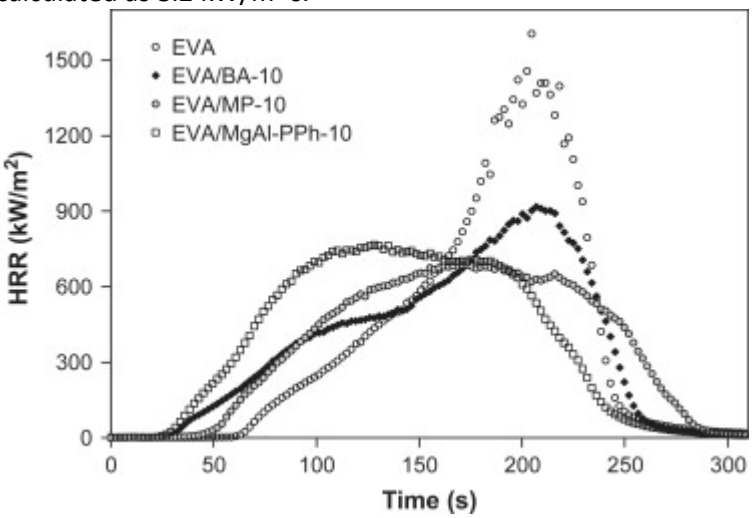

Fig. 10. Heat release rate curves neat EVA (empty circles), EVA/MP-10 (filled circles), EVA/BA-10 (filled diamonds), and EVA/MgAl–PPh-10 (empty squares) from cone calorimetry measurements at 35 kW/m^2.

Table 3. Cone calorimetry data for EVA and its composites at 35 kW/m^2.

Sample	**T_{ign} (s)**	**PHRR (kW/m^2) (% red)**	**t_{PHRR}(s)**	**THR (MJ/m^2)**	**AMLR (g/sm^2)**	**FPI (kW/m^{2}s)**	**FIGRA (kW/m^{2}s)**
EVA	65 ± 2	1680 ± 29	204 ± 8	124 ± 2	20 ± 2	26	8.2
EVA/BA-10	35 ± 5	899 ± 66(46)	207 ± 8	112 ± 2	16 ± 3	26	4.3
EVA/MP-10	47 ± 11	715 ± 47(57)	206 ± 28	112 ± 1	14 ± 4	15	3.4
EVA/MgAl–PPh-10	33 ± 3	793 ± 40(53)	140 ± 38	117 ± 1	17 ± 2	24	5.7
EVA/MgAl–PPh/MP/BA-2/4/4	29 ± 1	669 ± 34(60)	141 ± 10	114 ± 1	14 ± 1	23	4.7
EVA/MgAl–PPh/MP/BA-4/2/4	31 ± 4	680 ± 33(60)	140 ± 8	115 ± 2	15 ± 1	22	4.9
EVA/MgAl–PPh/MP/BA-4/4/2	30 ± 2	671 ± 8(60)	118 ± 6	114 ± 1	14 ± 1	22	5.7

T_{ign}, time-to-ignition; PHRR, peak heat release rate; (% red.), reduction in PHRR; t_{PHRR}, time to peak heat release rate; THR, total heat release; AMLR, average mass loss rate; FPI, fire performance index; FIGRA, fire growth rate.

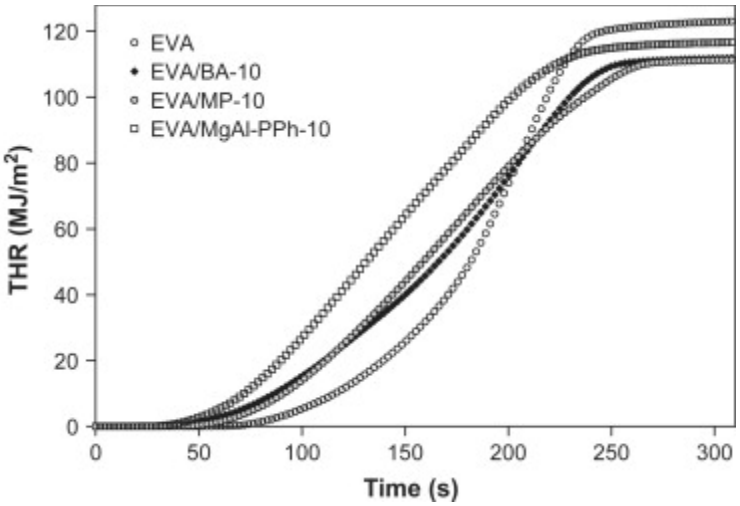

Fig. 11. The total heat release (THR) rate curves neat EVA (empty circles), EVA/MP-10 (filled circles), EVA/BA-10 (filled diamonds), and EVA/MgAl–PPh-10 (empty squares) from cone calorimetry measurements at 35 kW/m^2.

For EVA/BA-10 the HRR versus time curve is characterized by a shoulder from the time of sustained ignition, which is 35 s, up until after 150 s when a sharp peak centered at 207 s is observed. The PHRR value of EVA is reduced by about 46% from a value of 1680 to 899 kW/m^2 following the addition of boric acid. The calculated FPI value for EVA/BA-10 (26 kW/m^2 s) is the same as that calculated for EVA, while its FIGRA value is lower by a factor of two, Table 3. Despite the reduction in PHRR, there is no improvement in overall fire safety for EVA/BA-10 because the time-to-ignition is remarkably reduced upon addition of boric acid. However, once ignition occurs flame spread is slower for EVA/BA-10 when compared to EVA. A notable reduction in the THR value from 124 to 112 MJ/m^2 is observed following addition of boric acid. The inevitable production of heat resistant B_2O_3 and the release of water vapor during the decomposition of boric acid in the presence of EVA may be responsible for the observed reduction in both the PHRR and the THR. A ceramic-like B_2O_3 layer would slow mass and heat transfer to the pyrolysis zone while the water vapor produced would serve to quench the flame, hence reducing its intensity. The reduction in PHRR and THR can be linked to the observed reduction in the AMLR calculated as 16 g/s m^2.

The addition of MP significantly reduces the time-to-ignition from 65 to 47 s as well as the AMLR from 20 to 14 g/s m^2. There is a remarkable reduction in the PHRR value from 1680 to 715 kW/m^2 a 57% reduction with no change in the time it takes for the flame intensity to peak. The fire performance index (FPI), a parameter defined as the ratio of PHRR to time-to-ignition, is independent of the specimen geometry and can be used to evaluate the fire resistance of a material. The lower the FPI value the more fire safe a material is. The FPI value obtained for EVA is 26 kW/m^2 s while that determined for EVA/MP-10 is 15 kW/m^2 s suggesting that MP has a high flame retardant efficiency. These results are corroborated by an observed 58% reduction in the FIGRA value of EVA/MP-10. The THR value reported for EVA/MP-10 (112 MJ/m^2) is lower than observed for EVA (124 MJ/m^2) and this suggests that the amount of heat evolved during decomposition of the later is lower. The presence of MP may lead to the formation of a physical char layer that retards the flaming process via the retardation of mass transfer of combustibles and oxygen as well as heat penetration into the pyrolysis zone. Decomposition products from MP, such as melamine and NH_3, may lead to the dilution of the combustion atmosphere while the presence of phosphorus in the condensed phase promotes char formation; both of these events improve the flame retardancy of EVA composites [9].

The HRR versus time curve for EVA/MgAl–PPh-10 has a single plateau-like feature peaking at 793 kW/m^2 after 140 s. Addition of the phosphonate-intercalated hydrotalcite at 10% weight fraction leads to a 53% reduction in the PHRR and a slightly lower AMLR of 17 g/s m^2. The envisaged presence of phosphorus in the condensed phase inescapably offers a high possibility of phosphorus derivatives reacting with EVA resin to form more stable char networks with P–O–P and P–O–C linkages, as reported in the literature [28], [29]. These charred structures,

together with the release of water vapor and the possible catalytic role played by mixed Mg and Al oxides, are implicated in the reduction in PHRR and AMLR. There is no improvement in the fire resistance of EVA following addition of MgAl–PPh as indicated by a similar FPI value (24 kW/m^2 s) to that of EVA, however, the fire growth rate is lower for the former. The reduction in THR is lower than that observed following the addition of boric acid or melamine polyphosphate to EVA suggesting that MgAl–PPh is not as effective in reducing the amount of combustible matter produced during the flaming combustion process.

The concomitant effect of boric acid, melamine polyphosphate and MgAl–PPh on the flammability behavior of EVA in the samples, EVA/MgAl–PPh/MP/BA-2/4/4, EVA/MgAl–PPh/MP/BA-4/2/4, and EVA/MgAl–PPh/MP/BA-4/4/2 is also studied via cone calorimetry. Fig. 12 shows the heat release rate (HRR) versus time curves for EVA/MgAl–PPh/MP/BA-2/4/4, EVA/MgAl–PPh/MP/BA-4/2/4, and EVA/MgAl–PPh/MP/BA-4/4/2 while the data are presented in Table 3. The HRR profiles for these samples are similar within experimental error, all having a plateau-like resemblance with the PHRR values between 669 and 680 kW/m^2 after about 140 s. The observed PHRR values show an average 60% reduction when compared to that for EVA while the AMLR is reduced to an average of 14 g/s m^2. A reduction in THR from 124 to an average 114 MJ/m^2 is observed. A slight improvement in fire resistance as indicated by a reduction in the FPI value from 126 to an average of 122 kW/m^2 s is observed. The fire growth rate is remarkably reduced by the simultaneous addition of these potential fire retardants, Table 3.

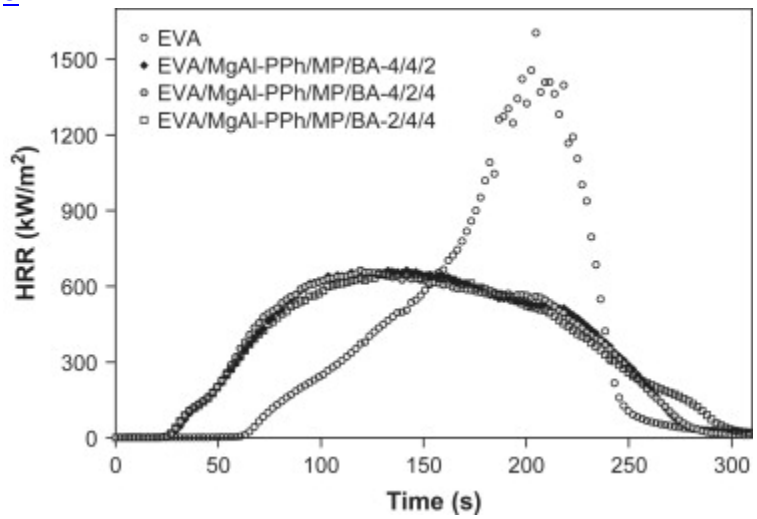

Fig. 12. Heat release rate curves for neat EVA (empty circles), EVA/MgAl–PPh/MP/BA-2/4/4 (empty squares), EVA/MgAl–PPh/MP/BA-4/2/4 (filled circles), and EVA/MgAl–PPh/MP/BA-4/4/2 (filled diamonds) from cone calorimetry measurements at 35 kW/m^2.

The percent reduction in the PHRR when the three additives are used simultaneously is about 60%. In order to assess possible chemical interactions between these additives or their decomposition products in enhancing the flame retardancy of EVA, expected reductions in PHRR for EVA/MgAl–PPh/MP/BA-2/4/4, EVA/MgAl–PPh/MP/BA-4/2/4, and EVA/MgAl–PPh/MP/BA-4/4/2 were calculated assuming that each of the additives would act independently. The calculated percent reductions were found to be 51, 52, and 53% for EVA/MgAl–PPh/MP/BA-2/4/4, EVA/MgAl–PPh/MP/BA-4/2/4, and EVA/MgAl–PPh/MP/BA-4/4/2 respectively. These values are lower than the experimentally observed values of 60% suggesting that the flame retardancy effect of the three additives when used together is more than mere additive, in fact this reflects synergism. The presence of Mg and Al metal oxides, together with phosphorus and boron may lead to the formation of highly flame retardant species, such as aluminum phosphate, boron phosphate, or boron–aluminum phosphate, which are very efficient physical and thermal barriers protecting the underlying polymers, according to the literature [29]. Other products from the decomposition of the additives, such as melamine, NH_3, and water, may in their own respect have changed the decomposition mechanism of EVA. While the simultaneous addition of three potential

flame retardants does not significantly reduce the total heat evolved or the average mass loss rate, the improvement in PHRR alone is equally important as it means a reduction in flame intensity.

4. Conclusions

EVA composites containing a layered phenyl phosphonate-intercalated inorganic/organic hybrid (MgAl–PPh), melamine polyphosphate, and boric acid were prepared via melt blending and their morphology evaluated using XRD and TEM. The inclusion of these potential flame retardant additives in EVA resulted in an improvement in the overall thermal stability and char formation. When MgAl–PPh was added at a 10% weight fraction the resultant EVA composite showed the greatest enhancement in thermal stability. The flammability behavior of flame retarded EVA composites was evaluated via cone calorimetry. Addition of MgAl–PPh, BA and MP at weight percent of 10% resulted in significant reductions in the time to sustained ignition and the peak heat release rate (PHRR) values. Similar reductions are observed for the average mass loss rate (AMLR) suggesting that the reductions in PHRR are due to the slower rate at which combustible volatiles are produced. However, the total heat evolved during combustion is not significantly affected by the presence of the additives. Synergistic interactions between the three flame retardants studied in this work may be responsible for more than additive flame retardancy effect observed with the reduction in PHRR when all these additives are used simultaneously.

Acknowledgements

Partial support of this work provided by the US Department of Commerce, National Institute of Standards and Technology, Fire Research Division under grant number 60NANBD6016 is gratefully acknowledged. The authors gratefully thank Dr Jeanne Hossenlopp and Dr Walid Awad for helpful discussions.

References

[1] S.K. Dutta, A.K. Bhownick, P.G. Mukunda, T.K. Chaki. **Thermal degradation studies of electron beam cured ethylene–vinyl acetate copolymer.** Polym Degrad Stab, 50 (1995), pp. 75-82

[2] F. Laoutid, L. Ferry, E. Leroy, J.M. Lopez Cuesta. **Intumescent mineral fire retardant systems in ethylene–vinyl acetate copolymer: effect of silica particles on char cohesion.** Polym Degrad Stab, 91 (2006), pp. 2140-2145

[3] D.-Y. Wang, X.-X. Cai, M.-H. Qu, Y. Liu, J.-S. Wang, Y.-Z. Wang. **Preparation and flammability of a novel intumescent flame-retardant poly(ethylene-co-vinyl acetate) system.** Polym Degrad Stab, 93 (2008), pp. 2186-2192

[4] S. Peeterbroeck, M. Alexandre, J.B. Nagy, C. Pirlot, A. Fonseca, N. Moreau, *et al.* **Polymer-layered silicate–carbon nanotube nanocomposites: unique nanofiller synergistic effect.** Compos Sci Technol, 64 (2004), pp. 2317-2323

[5] F. Fengge Gao, G. Beyer, Q. Yuan. **A mechanistic study of fire retardancy of carbon nanotube/ethylene vinyl acetate copolymers and their clay composites.** Polym Degrad Stab, 89 (2005), pp. 559-564

[6] M. Alexandre, P. Dubois. **Polymer-layered silicate nanocomposites: preparation, properties and uses of a new class of materials.** Mater Sci Eng R Reports, 28 (2000), pp. 1-63

[7] Zhang J, Hereid J, Hagen M, Bakirtzis D, Delichatsios MA. Effects of nanoclay and fire retardants on fire retardancy of a polymer blend of EVA and LDPE. Fire Safety J, in press. doi:10.1016/j.firsaf.2008.10.005.

[8] C. Baillet, L. Delfosse. **The combustion of polyolefins filled with metallic hydroxides and antimony trioxide.** Polym Degrad Stab, 30 (1990), pp. 89-99

[9] L. Ye, B. Qu. **Flammability characteristics and flame retardant mechanism of phosphate-intercalated hydrotalcite in halogen-free flame retardant EVA blends.** Polym Degrad Stab, 93 (2008), pp. 918-924

[10] G. Zhang, P. Ding, M. Zhang, B. Qu. **Synergistic effects of layered double hydroxide with hyperfine magnesium hydroxide in halogen-free flame retardant EVA/HFMH/LDH nanocomposites.** Polym Degrad Stab, 92 (2007), pp. 1715-1720

[11] L. Du, B. Qu, Z. Xu. **Flammability characteristics and synergistic effect of hydrotalcite with microencapsulated red phosphorus in halogen-free flame retardant EVA composite.** Polym Degrad Stab, 91 (2006), pp. 995-1001
[12] G. Camino, A. Maffezzoli, M. Braglia, M. De Lazzaro, M. Zammarano. **Effect of hydroxides and hydroxycarbonate structure on fire retardant effectiveness and mechanical properties in ethylene–vinyl acetate copolymer.** Polym Degrad Stab, 74 (2001), pp. 457-464
[13] E.D. Dimotakis, T.J. Pinnavaia. **New route to new layered double hydroxides intercalated by organic anions: precursors to polyoxometalate-pillared derivatives.** Inorg Chem, 29 (1990), pp. 2393-2394
[14] D. Wang, J. Zhu, Q. Yao, C.A. Wilkie. **A comparison of various methods for the preparation of polystyrene and poly(methyl methacrylate) clay nanocomposites.** Chem Mater, 14 (2002), pp. 3837-3843
[15] F.R. Costa, A. Leuteritz, U. Wagenknecht, D. Jehnichen, L. Häußler, G. Heinrich. **Intercalation of Mg–Al layered double hydroxide by anionic surfactants: preparation and characterization.** Appl Clay Sci, 27 (2004), pp. 159-177
[16] H. Nijs, A. Clearfield, E.F. Vansant. **The intercalation of phenyl phosphonic acid in layered double hydroxides..** Microporous Mesoporous Mater, 23 (1998), pp. 97-108
[17] C. Nyambo, E. Kandare, D. Wang, C.A. Wilkie. **Flame-retarded polystyrene: investigating chemical interactions between ammonium polyphosphate and MgAl layered double hydroxide.** Polym Degrad Stab, 93 (2008), pp. 1656-1663
[18] C. Nyambo, P. Songtipya, E. Manias, M. Jimenez–Gasco, C.A. Wilkie. **Effect of MgAl-layered double hydroxide exchanged with linear alkyl carboxylates on fire retardancy of PMMA and PS.** J Mater Chem, 28 (2008), pp. 4827-4838
[19] C. Nyambo, D. Wang, C.A. Wilkie. **Will layered double hydroxides give nanocomposites with polar or non-polar polymers?** Polym Adv Technol (2008) doi:10.1002/pat.1272
[20] S. Bourbigot, S. Duquesne. **Fire retardant polymers: recent developments and opportunities.** J Mater Chem, 17 (2007), pp. 2283-2300
[21] L. Costa, G. Camino. **Thermal behavior of melamine.** J Therm Anal, 34 (1988), pp. 423-429
[22] S. Jahromi, W. Gabriëlse, A. Braam. **Effect of melamine polyphosphate on thermal degradation of polyamides: a combined X-ray diffraction and solid-state NMR study.** Polymer, 44 (2003), pp. 25-37
[23] M. Jimenez, S. Duquesne, S. Bourbigot. **Intumescent fire protective coating: toward a better understanding of their mechanism of action.** Thermochim Acta, 449 (2006), pp. 16-26
[24] M. Zanetti, G. Camino, R. Thomann, R. Mülhaupt. **Synthesis and thermal behaviour of layered silicate–EVA nanocomposites.** Polymer, 42 (2001), pp. 4501-4507
[25] A. Riva, G. Camino, L. Fomperie, P. Amigouët. **Fire retardant mechanism in intumescent ethylene vinyl acetate compositions.** Polym Degrad Stab, 82 (2003), pp. 341-346
[26] M. Zanetti, T. Kashiwagi, L. Falqui, G. Camino. **Cone calorimeter combustion and gasification studies of polymer layered silicate nanocomposites.** Chem Mater, 14 (2002), pp. 881-887
[27] M.C. Costache, D.D. Jiang, C.A. Wilkie. **Thermal degradation of ethylene–vinyl acetate copolymer nanocomposites.** Polymer, 46 (2005), pp. 6947-6958
[28] Q. Wu, J. Lu, B. Qu. **Preparation and characterization of microcapsulated red phosphorous and its flame-retardant mechanism in halogen-free flame retardant polyolefins.** Polym Int, 52 (2003), pp. 1326-1331
[29] U. Braun, B. Schartel, M.A. Fichera, C. Jäger. **Flame retardancy mechanisms of aluminum phosphinate in combination with melamine polyphosphate and zinc borate in glass–fibre reinforced polyamide 6,6.** Polym Degrad Stab, 92 (2007), pp. 1528-1545